



Original Article

Optical Properties of S-doped and S, N Co-doped Graphene Quantum Dots and Application

Pham Thu Nga^{1,2}, Trinh Thi Hue^{1,2}, Nguyen Thi Mai Huong³,
Phan Xuan Thien³, Le Xuan Hung^{2,4,*}

¹*Institute of Theoretical and Applied Research, Duy Tan University,
01 Phung Chi Kien, Cau Giay, Hanoi, Vietnam*

²*Duy Tan University, 03 Quang Trung, Hai Chau, Da Nang, Vietnam*

³*Institute of Physics, Vietnam Academy of Science and Technology,
18 Hoang Quoc Viet, Cau Giay, Hanoi, Vietnam*

⁴*Institute of Research and Development, Duy Tan University, 03 Quang Trung, Hai Chau, Da Nang, Vietnam*

Received 17th June 2024

Revised 26th December 2024; Accepted 26th December 2024

Abstract: In recent years, carbon-based quantum dots, including carbon quantum dots (CQDs) and graphene quantum dots (GQDs), have been widely researched as new alternatives to conventional antibacterial agents. The structural characteristics and properties of the materials can also be tuned and controlled by changing the shape and size of the GQDs. Effective doping with heteroatoms can also tune the optical, electronic and electrochemical properties, etc., of GQDs. In this report, we study and synthesize sulfur (S)-doped graphene quantum dots and sulfur (S), nitrogen (N)-co-doped-graphene quantum dots using a simple method that requires minimal energy and is environmentally friendly. By controlling the absorption and luminescence spectra in the desired wavelength range, S, N-GQDs can easily be applied as biocides for common bacteria such as *E. coli* and *S. aureus*, also presented in this report.

Keywords: Doped-GQDs, S-GQDs, S, N-GQDs, absorption, photoluminescence spectra, antibacterial.

1. Introduction

In contrast to amorphous and spherical carbon dots, graphene quantum dots (GQDs) exhibit a flat, planar structure with a graphene

core that features sp^2 hybridization and is surrounded by edges. Typically, GQDs have lateral sizes around 10 nm or less and consist of 1–5 layers. This configuration leads to the behavior of the quantum confinement effect as their dimensions are smaller than the exciton Bohr radius [1]. GQDs also have a high absorption coefficient ($\sim 10^5 \text{ cm}^{-1}$), allowing

* Corresponding author.

E-mail address: lexuanhung@duytan.edu.vn

<https://doi.org/10.25073/2588-1140/vnunst.5757>

them to absorb photons more efficiently and facilitate electron transport to the conduction band [1, 2]. Their structural design, which includes a large surface area and numerous edges, renders them highly reactive. Additionally, introducing functional groups during synthesis can impart hydrophilic properties to the otherwise hydrophobic graphene planes. The physicochemical properties of GQDs are subject to change depending on the synthesis method used. Therefore, a thorough understanding of the characteristics of GQDs is crucial before delving into their synthesis and applications. Moreover, the optical properties of GQDs can be tailored by doping them with various atoms, including those other than carbon. Using heteroatoms in GQDs is an effective strategy to adjust their electronic structure and surface characteristics, thus opening up various application possibilities. Some of the potential applications of this material include biomedical labeling [3-5], antibacterial agents [6-8], optical visualization [1, 3], solar cells [9-11], environmental treatment [12, 13], and optoelectronic devices [14, 15]. Many published works have been on doping different types of elements into this material (such as N, S, B, Cl, and F). Among these, doping S into GQDs is proven difficult because the size of an S atom is much larger than that of a C atom [16].

Graphene quantum dots (GQDs) have garnered significant attention due to their unique electronic and physicochemical properties. Notably, their excellent electron transport capabilities grant them peroxidase-like activity. Furthermore, GQDs can inhibit bacterial growth through photothermal effects or by physically disrupting bacterial structures when in the form of sheets. Nonetheless, the antibacterial efficacy of GQDs often relies heavily on substrates or light, which limits their practical applications. To overcome these limitations, it is crucial to investigate other antibacterial mechanisms to inspire the development of multi-target antibacterial GQDs. Research has explored the impact of

GQDs on microbial morphology, reactive oxygen species (ROS) production, and alterations in protein, nucleic acid, and ATP levels [2].

This report presents the synthesis method of S-GQDs and S, N-GQDs, along with their related properties, are presented. S-GQDs and S, N-GQDs were fabricated by microwave pyrolysis, followed by hydrothermal treatment in NaOH solution. This is an environmentally friendly method. Besides, the precursors are cheap, easily obtainable, and non-toxic substances. This research aims to detail the effects of doping on structural properties, crystal quality, and photoluminescence properties. The formation and morphology of S-GQDs and S, N-GQDs will be studied using HR-TEM and XPS images. The optical properties of the fabricated doped-GQDs will be analyzed via absorption and fluorescence spectroscopy. The antibacterial activity of doped GQDs is also presented, demonstrating their potential application.

2. Experimental

2.1. Fabrications of S-GQDs and S, N-GQDs

S-GQDs were synthesized by pyrolysis combined with a hydrothermal process using citric acid (CA) and 3-mercaptopropionic acid (MSA) as precursors of carbon (C) and sulfur (S). Specifically, CA and MSA were weighed according to the calculated ratio and placed in a heat-resistant beaker for pyrolysis by microwave oven for 4 minutes with the capacity of 500 W. After liquefaction and turning to the color of cockroach wings, the solution was quickly dripped into a pre-prepared 1.2% NaOH solution. The resulting solution was placed in an autoclave and hydrothermally heated at 200 °C for 4 hour. The manufacturing process is depicted in Figure 1. S, N-GQDs samples were prepared using a similar method, combining microwave pyrolysis with hydrothermal, using citric acid as C and thiourea as S and N source. The preparation process is similar to that described in the

publication cited as reference no. [17]. Conditions for preparing S, N-GQDs samples included pyrolysis of CA and thiourea molten mixture in a microwave oven, operating at

500 W for 4 min, followed by hydrothermal treatment in 100 ml of 1.2 wt% NaOH solution (or in water) in an oven at 200 °C for 4 hours. The CA/thiourea mole ratio is 1/4.

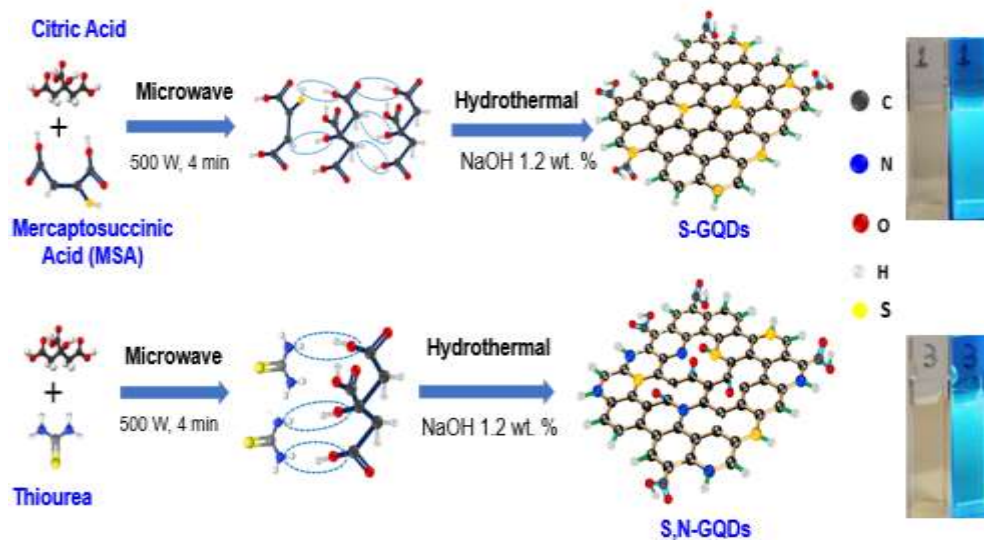


Figure 1. Schematic for fabrication of S-GQDs and S, N-GQDs. Images on the right side show the color and fluorescence characteristics of the synthesized samples.

2.2. Characterization of S-GQDs and S, N-GQDs

The morphology and size distribution of the doped-GQDs samples were characterized using a JEOL JEM-2100 high-resolution transmission electron microscope (HRTEM) at an accelerating voltage of 200 kV. To determine the content of the atom % of N, S, O, and C and the bonds in the samples, X-ray photoelectron spectroscopy (XPS) was performed using a Thermo Fisher (model NX10). The ultraviolet-visible (UV-Vis) absorption spectra of the prepared samples in water were measured in the wavelength range of 200–1100 nm using a Cary 60 UV-Vis spectrophotometer (Agilent). The PL spectra were carried out on a Fluorolog-322 system (Horiba Jobin-Yvon) using a 450 W Xenon light with an excitation wavelength of 360 nm.

2.3. Antibacterial Activity Assessments

The antibacterial activity of S, N-GQDs was examined at the Quality Assurance and

Testing Center 1 (Quartest 1), Vietnam Directorate for Standards, Metrology, and Quality, using two strains of *E. coli* and *S. aureus* bacteria. The culture and storage of these two bacteria strains followed the verified procedures of the Quality Assurance and Testing Center 1. The antibacterial test was carried out in the laboratory at room temperature and under light by the following process: i) Prepare a control sample by taking 10 ml of sterile distilled water and adding *E. coli* (or *S. aureus*) strain enrichment broth; ii) Prepare the test sample by taking 10 ml of S, N-GQDs solution and adding *E. coli* (or *S. aureus*) strain enrichment broth. The test and control samples were shaken evenly to increase the interaction between our fabricated samples and bacterial strains. Samples were analyzed independently. The plate counting method was used to evaluate the antibacterial activity of N-GQDs and S, N-GQDs by determining the number of colony-forming units (CFU) on the agar plate after 5 mins.

The bactericidal efficiency R (%) was calculated according to the following formula [2, 18]:

$$R = \frac{N1 - N2}{N1} \times 100\%$$

In there:

$N1$ is the test microbial density of the control after 5 min (CFU/mL), and $N2$ density of live micro-organisms of the test sample after 5 min exposure time (CFU/mL).

3. Results and Discussions

3.1. Morphology and Bonding Characteristics of S-GQDs and S,N-GQDs

XPS analysis was performed to determine the elemental composition of the fabricated samples. The XPS spectrum (in Figure 2) for S, N-GQDs reveals that the C 1s peak, primarily corresponding to graphene, is located at 285.1 eV, while the O 1s peak is at 531.9 eV, as reported by [19, 20]. The peaks around 400 and 163.2 eV in the full spectrum are also attributed to N 1s and S 2p, respectively. A Na peak was also detected at 496.9 eV [21]. The fact that the O 1s peak is higher than the C 1s peak, along with the presence of Na, suggests redox reactions can occur during hydrothermal process. In the case of S-GQDs, the C 1s peak is located at 284.8 eV, and the O 1s peak at 531.9 eV. Peaks observed at 164.0 and 168.6 eV are assigned to S 2p, with a Na peak also appearing at 496.9 eV, similar to the S, N-GQDs. The XPS survey confirms the presence of C, O, N and S in S, N-GQDs, with at % of 57.35%, 32.25%, 7.7% and 2.69%, respectively. For S-GQDs, the at % of C, O, and S were 75.2%, 20.2%, and 4.6%, respectively. The above results indicate that S and N atoms were incorporated into the graphene lattice, forming corresponding bonds.

Morphology of S-GQDs and S, N-GQDs by TEM images: The size and shape of the S-GQDs and S, N-GQDs samples were observed through TEM images. TEM images of S-GQDs and S, N-GQDs samples synthesized by pyrolysis combined with hydrothermal are

shown in Figure 3. The average size of the S-GQDs samples is about 3.7 nm, while the S, N-GQDs samples have an average size of 8.3 nm. The particle size of the S-GQDs is not uniformly distributed, ranging from 3 nm to 5 nm. However, the S, N-GQDs sample exhibits a fairly uniform size distribution and the particles are clustered quite well. A possible explanation is that many residual substances during the fabrication process, make the particles stick together. Therefore, the additional use of a hydrothermal process will push the reaction to continue, resulting in a more uniform particle size distribution.

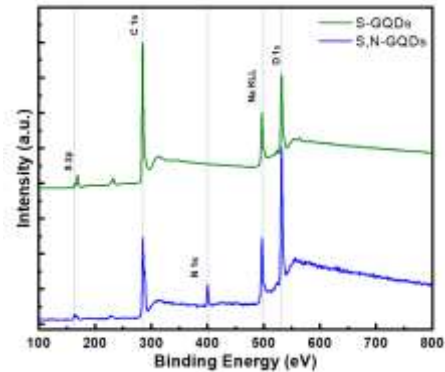


Figure 2. XPS spectra of S-GQDs and S,N-GQDs samples.

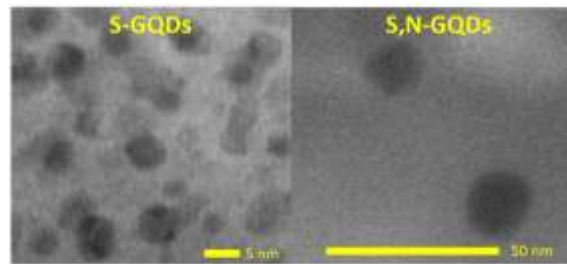


Figure 3. TEM images of S-GQDs (left) and S, N-GQDs (right) samples.

3.2. Optical Properties of S-GQDs and S,N-GQDs.

After fabrication, the samples were confirmed to be GQDs with S-doping or S, N co-doping and were investigated for their optical properties through absorption and fluorescence measurements. Figure 4 shows the

absorption spectra of GQDs, S-GQDs, and S, N-GQDs samples. We can see that the absorption spectrum of the GQDs sample has only one shoulder at about 265 nm, related to the $\pi \rightarrow \pi^*$ transition state at sp^2 of carbon atoms. For the S-GQDs and S, N-GQDs samples, absorption bands are located at 340 nm and 332 nm, respectively, which characterize the $C\pi \rightarrow O\pi^*$ transition formed when doping with S and N. In addition, the absorption peak of the S-GQDs sample has relatively low intensity compared to the S, N-GQDs sample. This can be explained as follows: the absorption band at 332-340 nm characterizes the $C\pi \rightarrow O\pi^*$ [22] electron transfer. By co-doping S and N, many bonds containing C=O groups are formed, leading to a high absorption peak at this range compared to the S-only doped sample. This result is also consistent with published results [23].

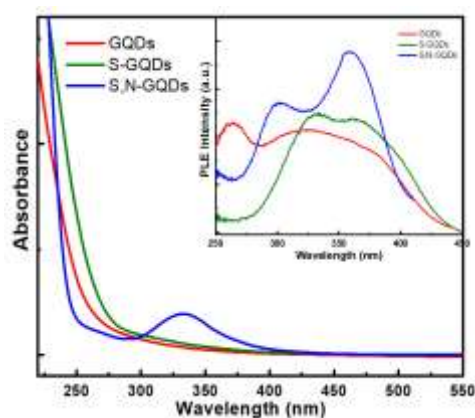


Figure 4. Absorption spectra of S-GQDs and S, N-GQDs samples. Inset are the PLE spectra of these.

The photoluminescence spectra of the GQDs and doped GQDs samples are shown in Figure 5. From Figure 5, it is evident that the fluorescence spectrum of the samples has a broadband shape with a red-shifted emission peak when doped (inset in Figure 5). The luminescence intensity increases significantly upon doping and is most significant when co-doped with S and N. The photoluminescence excitation (PLE) spectra are also presented in the inset of Figure 4. For the pure GQDs

sample, the PLE peak appears at 265 nm, alongside a wide PLE band from 300 to 400 nm. When doping with S or co-doping S and N, the PLE peaks shift to longer wavelengths: 330 nm for the S-GQDs sample and 300 nm for the S, N-GQDs samples. Additionally, two extra PLE peaks appear at 363 nm for the S-GQDs samples and 358 nm for the S, N-GQDs sample. To explain the absorption and emission mechanisms and the changes in the position of the maximum emission band and its intensity according to the excitation wavelength, we refer to the energy levels diagram and electron transfer according to reference no. [22]. Accordingly, impurities create additional energy levels between the $C\pi$ and $C\pi^*$ levels, and $O\pi^*$ states also appear. The formation of these states causes the fluorescence spectra to shift to longer wavelengths [22, 24, 25]. Simultaneously, their luminescence intensity also increases. The dopant concentration increases when co-doping with S and N, leading to enhanced fluorescence. This result is consistent with published findings [23, 26-28].

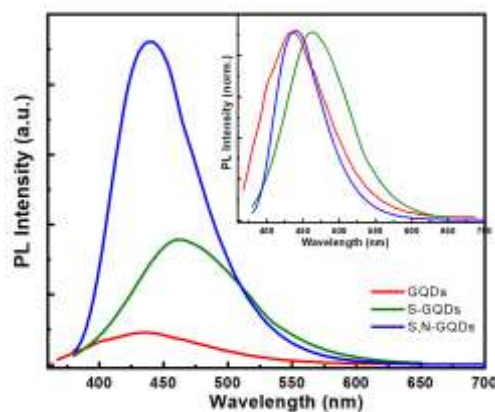


Figure 5. PL spectra of S-GQDs and S, N-GQDs samples under 360 nm excitation. Inset are the PL normalized spectra of these.

3.3. Antibacterial Activity of S, N-GQDs.

In this study, we evaluated the antibacterial properties of the synthesized material by subjecting it to antibacterial tests after fabrication. The samples were exposed to specific bacterial strains, and their ability to

inhibit bacterial growth was analyzed. Among the materials, we chose S, N-GQDs for testing because previous studies suggest that doping GQDs with sulfur (S) and nitrogen (N) significantly enhances antibacterial activity [29, 30]. This is due to increased reactive oxygen species (ROS) production, which disrupts bacterial cell membranes. S, N-GQDs thus show great potential for biomedical and antimicrobial applications.

The antibacterial activity of S, N-GQDs was explored against *E. coli* and *S. aureus*. Figure 6 shows images of colonies obtained after treatment with different concentrations of S, N-GQDs under the same ambient conditions. This demonstrates that S, N-GQDs performed excellent antibacterial activity against *E. coli* with a bactericidal efficiency of 99.21%. However, for *S. aureus* bacteria, the fabricated S, N-GQDs sample showed a lower efficiency, achieving only 14.28%. Our results also indicate that S, N-GQDs kill *E. coli* strains more efficiently than *S. aureus*. The antibacterial ability of S, N-GQDs is attributed to the antibacterial activity of the C=O and -COOH functional groups in the doped GQDs. According to recent publications [2, 31], due to

the presence of C=O and -COOH functional groups, the antibacterial mechanisms when GQDs are doped can occur as follows:

i) could cause generate ROS leading to oxidative stress in bacteria; ii) acidic doped GQDs entering bacterial cells and disrupting the intracellular pH balance; iii) binding to membranes or wall and affecting their integrity; iv) linking to nucleic acids through hydrogen bonding and the π - π configuration, interfering with nucleic acid synthesis; and v) preventing energy metabolism pathways, causing a decline in ATP production. For gram-positive bacteria, the antibacterial activity of materials is related mainly to electrostatic interactions of cationic molecules with the bacterial cell surface [31]. In this report, the bactericidal efficiency of S, N-GQDs against *S. aureus* bacteria (Gram-positive) is much lower than that against *E. coli* bacteria (Gram-negative), suggesting that the electrostatic interaction of S, N-GQDs with the cell surface is not strong, or it may be related to differences in the composition of the cell wall of the two bacterial strains [31].

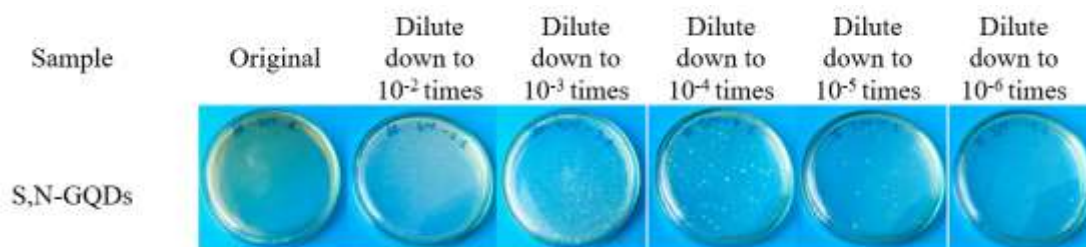


Figure 6. Representative culture images of colonies after receiving treatments with various concentrations of S, N-GQDs aqueous solutions.

4. Conclusion

In summary, the fabrication of S-GQDs and S, N-GQDs was initially successful using citric acid (CA). By combining pyrolysis using a microwave oven with a hydrothermal process, we have produced doped GQDs with more uniform size: the average size of the S-GQDs sample is about 3.7 nm, and the S, N-GQDs

sample is 8.3 nm. The absorption and fluorescence of doped GQDs are not only related to the $C\pi \rightarrow C\pi^*$ transitions but also to the $C\pi \rightarrow O\pi^*$ transitions and states related to surface states. The antibacterial activity of S, N-GQD sample was tested against two types of bacteria, *E. coli* and *S. aureus*, and was found to be more effective in killing *E. coli*, with a bactericidal efficiency of 99.21%.

Acknowledgements

This research is funded by Vietnam National Foundation for Science and Technology Development (NAFOSTED) under grant number 103.03-2020.22.

References

- [1] H. Cho, G. Bae, B. H. Hong, Engineering Functionalization and Properties of Graphene Quantum Dots (GQDs) with Controllable Synthesis for Energy and Display Applications, *Nanoscale*, Vol. 16, No. 7, 2024, pp. 3347-3378.
- [2] W. Wu, Y. Qin, Y. Fang, Y. Zhang, S. Shao, F. Meng, M. Zhang, Based on Multi-omics Technology Study the Antibacterial Mechanisms of pH-dependent N-GQDs Beyond ROS, *J. Hazard Mater*, Vol. 441, 2023, pp. 129954.
- [3] Y. Yan, J. Gong, J. Chen, Z. Zeng, W. Huang, K. Pu, J. Liu, P. Chen, Recent Advances on Graphene Quantum Dots: From Chemistry and Physics to Applications, *Adv Mater*, Vol. 31, No. 21, 2019, pp. e1808283.
- [4] G. Perini, V. Palmieri, G. Ciasca, M. De Spirito, M. Papi, Unravelling the Potential of Graphene Quantum Dots in Biomedicine and Neuroscience, *Int J. Mol Sci*, Vol. 21, No. 10, 2020, pp. 3712-3736.
- [5] K. Jin, H. Gao, L. Lai, Y. Pang, S. Zheng, Y. Niu, X. Li, Preparation of Highly Fluorescent Sulfur Doped Graphene Quantum Dots for Live Cell Imaging, *Journal of Luminescence*, Vol. 197, 2018, pp. 147-152.
- [6] B. C. Lee, J. Y. Lee, J. Kim, J. M. Yoo, I. Kang, J. J. Kim, N. Shin, D. J. Kim, S. W. Choi, D. Kim, B. H. Hong, K. S. Kang, Graphene Quantum Dots as Anti-inflammatory Therapy for Colitis, *Sci. Adv.*, Vol. 6, 2020, pp. 2630.
- [7] S. Chen, Y. Quan, Y. L. Yu, J. H. Wang, Graphene Quantum Dot/Silver Nanoparticle Hybrids with Oxidase Activities for Antibacterial Application, *ACS Biomaterials Science & Engineering*, Vol. 3, No. 3, 2017, pp. 313-321.
- [8] S. Kadian, G. Manik, N. Das, P. Nehra, R. P. Chauhan, P. Roy, Synthesis, Characterization and Investigation of Synergistic Antibacterial Activity and Cell Viability of Silver-sulfur Doped Graphene Quantum Dot (Ag@S-GQDs) Nanocomposites, *J. Mater Chem B*, Vol. 8, No. 15, 2020, pp. 3028-3037.
- [9] V. D. Dao, P. Kim, S. Baek, L. L. Larina, K. Yong, R. Ryoo, S. H. Ko, H. S. Choi, Facile Synthesis of Carbon Dot-Au Nanoraspberries and Their Application as High-performance Counter Electrodes in Quantum Dot-sensitized Solar Cells, *Carbon*, Vol. 96, 2016, pp. 139-144.
- [10] Y. Zhu, C. Dai, C. Hao, H. Guo, L. Yan, Purification of Nitrogen-doped Graphene Quantum Dots and its Application in Polymer Solar Cells, *Colloids and Surfaces A: Physicochemical and Engineering Aspects*, Vol. 648, 2022.
- [11] T. Majumder, S. Dhar, P. Chakraborty, K. Debnath, S. P. Mondal, S. N Co-Doped Graphene Quantum Dots Decorated C-Doped ZnO Nanotaper Photoanodes for Solar Cells Applications, *Nano*, Vol. 14, No. 01, 2019.
- [12] R. M. Rezaei, M. Jaymand, Graphene Quantum Dots Coated on Quartz Sand as Efficient and Low-cost Adsorbent for Removal of Hg²⁺ and Pb²⁺ from Aqueous Solutions, *Environmental Progress & Sustainable Energy*, Vol. 38, No. S1, 2018.
- [13] N. A. Tran, N. T. Hien, N. M. Hoang, H. L. T. Dang, D. Q. Huy, T. V. Quy, N. T. Hanh, N. H. Vu, V. D. Dao, Carbon Dots in Environmental Treatment and Protection Applications, *Desalination*, Vol. 548, No., 2023.
- [14] D. I. Son, B. W. Kwon, D. H. Park, W. S. Seo, Y. Yi, B. Angadi, C. L. Lee, W. K. Choi, Emissive ZnO-graphene Quantum Dots for White-light-emitting Diodes, *Nat Nanotechnol*, Vol. 7, No. 7, 2012, pp. 465-71.
- [15] F. Khan, J. H. Kim, Emission-wavelength-Dependent Photoluminescence Decay Lifetime of N-functionalized Graphene Quantum Dot Downconverters: Impact on Conversion Efficiency of Cu(In, Ga)Se₂ Solar Cells, *Sci Rep*, Vol. 9, No. 1, 2019, pp. 10803.
- [16] S. Kang, Y. K. Jeong, K. H. Jung, Y. Son, W. R. Kim, J. H. Ryu, K. M. Kim, One-step Synthesis of Sulfur-incorporated Graphene Quantum Dots using Pulsed Laser Ablation for Enhancing Optical Properties, *Opt Express*, Vol. 28, No. 15, 2020, pp. 21659-21667.
- [17] L. X. Hung, N. H. Yen, T. T. Hue, D. N. Thuan, P. N. Thang, V. T. H. Hanh, V. C. Nhung, J. Laverdant, N. T. M. Huong, P. T. Nga, Fabrication and Optical Properties of Sulfur- and Nitrogen-doped Graphene Quantum Dots by the Microwave-hydrothermal Approach, *Journal of Nanoparticle Research*, Vol. 24, No. 10, 2022, pp. 206.
- [18] H. Liu, N. Yang, D. Teng, R. Mao, Y. Hao, X. Ma, X. Wang, J. Wang, Fatty Acid Modified-antimicrobial Peptide Analogues with Potent

- Antimicrobial Activity and Topical Therapeutic Efficacy Against *Staphylococcus Hyicus*, *Appl Microbiol Biotechnol*, Vol. 105, No. 14-15, 2021, pp. 5845-5859.
- [19] W. Zhu, X. Feng, M. Zhao, Z. Wei, Z. Liu, G. Wang, Q. Guo, D. Chen, Scalable and Atom Economic Preparation of Red-near-infrared Emitted N-doped Graphene Quantum Dots with a High Quantum Yield, *Diamond and Related Materials*, Vol. 116, 2021, pp. 108395.
- [20] K. Vrettos, P. Angelopoulou, J. Papavasiliou, G. Avgouropoulos, V. Georgakilas, Sulfur-doped Graphene Aerogels Reinforced with Carbon Fibers as Electrode Materials, *Journal of Materials Science*, Vol. 55, No. 23, 2020, pp. 9676-9685.
- [21] Y. Li, Y. Hu, Y. Zhao, G. Shi, L. Deng, Y. Hou, L. Qu, An Electrochemical Avenue to Green-luminescent Graphene Quantum Dots as Potential Electron-acceptors for Photovoltaics, *Adv Mater*, Vol. 23, No. 6, 2011, pp. 776-80.
- [22] T. V. T. Nhung, H. V. Tuyen, N. Tran, L. X. Hung, S. N Co-doped Graphene Quantum Dots Fabricated by Rapid Microwave-assisted Pyrolysis and Their Optical Properties, *Materials Today Communications*, Vol. 37, 2023, pp. 107282.
- [23] S. Kadian, G. Manik, A Highly Sensitive and Selective Detection of Picric Acid using Fluorescent Sulfur-doped Graphene Quantum Dots, *Luminescence*, Vol. 35, No. 5, 2020, pp. 763-772.
- [24] P. R. Kharangarh, S. Umapathy, G. Singh, Thermal Effect of Sulfur Doping for Luminescent Graphene Quantum Dots, *ECS Journal of Solid State Science and Technology*, Vol. 7, No. 3, 2018, pp. M29-M34.
- [25] P. R. Kharangarh, S. Umapathy, G. Singh, Investigation of Sulfur Related Defects in Graphene Quantum Dots for Tuning Photoluminescence and High Quantum Yield, *Applied Surface Science*, Vol. 449, 2018, pp. 363-370.
- [26] S. Kadian, G. Manik, K. Ashish, M. Singh, R. P. Chauhan, Effect of Sulfur Doping on Fluorescence and Quantum Yield of Graphene Quantum Dots: An Experimental and Theoretical Investigation, *Nanotechnology*, Vol. 30, No. 43, 2019, pp. 435704.
- [27] Y. Dong, J. Shao, C. Chen, H. Li, R. Wang, Y. Chi, X. Lin, G. Chen, Blue Luminescent Graphene Quantum Dots and Graphene Oxide Prepared by Tuning the Carbonization Degree of Citric Acid, *Carbon*, Vol. 50, No. 12, 2012, pp. 4738-4743.
- [28] X. Li, S.P. Lau, L. Tang, R. Ji, P. Yang, Sulphur Doping: A Facile Approach to Tune the Electronic Structure and Optical Properties of Graphene Quantum Dots, *Nanoscale*, Vol. 6, No. 10, 2014, pp. 5323-5328.
- [29] M. D. R. Andrade, T. A. Nguyen, W. P. Mistler, J. Armas, J. E. Lu, G. Roseman, W. R. Hollingsworth, F. Nichols, G. L. Millhauser, A. Ayzner, C. Saltikov, S. Chen, Antimicrobial Activity of Graphene Oxide Quantum Dots: Impacts of Chemical Reduction, *Nanoscale Adv*, Vol. 2, No. 3, 2020, pp. 1074-1083.
- [30] A. Ananthanarayanan, Y. Wang, P. Routh, M. A. Sk, A. Than, M. Lin, J. Zhang, J. Chen, H. Sun, P. Chen, Nitrogen and Phosphorus Co-doped Graphene Quantum Dots: Synthesis from Adenosine Triphosphate, Optical Properties, and Cellular Imaging, *Nanoscale*, Vol. 7, No. 17, 2015, pp. 8159-65.
- [31] N. A. Travlou, D. A. Giannakoudakis, M. Algarra, A. M. Labella, E. R. Castellón, T. J. Bandoz, S- and N-doped Carbon Quantum Dots: Surface Chemistry Dependent Antibacterial Activity, *Carbon*, Vol. 135, 2018, pp. 104-111.